ADVANCED SUSTAINABLE SYSTEMS
www.advsustainsys.com

Pressure Dependence of the Low Temperature Carbonation Kinetics of Calcium Oxide for Potential Thermochemical Energy Storage Purposes and Sustainable CO_2 Fixation

Georg Gravogl, Felix Birkelbach, Danny Müller, Christian L. Lengauer, Peter Weinberger, and Ronald Miletich**

The pressure effect on the carbonation behavior of CaO as model compound is studied under mild hydrothermal conditions, as relevant to sustainable geological CO_2 sequestration and for potential utilization in thermochemical energy storage. Reaction yields are determined experimentally by means of in situ powder X-ray diffraction using CaO powder samples in a controlled reaction with CO_2 under gas pressures between 1.0 and 5.0 MPa and at temperatures between 298 and 373 K. The results show a two-step conversion of CaO to $CaCO_3$, involving $Ca(OH)_2$ as a reactive intermediate, with differing influences of the microstructures on the individual reaction sub-steps. A kinetic evaluation of the experimental data delivers a high rate-enhancing effect of temperature on the hydration reaction, whereas the $CaCO_3$ formation is strongly dependent on the available CO_2 gas pressure. With this systematic investigation the optimal pressure and temperature conditions for this reaction system can be determined delivering a contribution to a sustainable climate and energy management.

1. Introduction

Global carbon dioxide (CO_2) emissions are seen as the main driving force of human-induced climate changes and need to be reduced to meet climate goals. Combustion processes liberating CO_2 are currently insufficiently decreased, thus carbon capture and storage (CCS) is becoming increasingly important. In general, CO_2 degradation, long-term sequestration, and conversion into polymerized species with larger building blocks are the most promising strategies. Also more specific approaches as recently exemplified in artificial photosynthesis[1] or microbial fixation[2] are highly awarded, although offering yet only minor contributions for reducing anthropogenic emissions. Sequestration of CO_2 in geological formations is the most mature technology, applicable on large scales. Captured CO_2 introduced into saline aquifers,[3,4] nonmineable coalbeds,[5,6] or depleted hydrocarbon reservoirs[7–9] is permanently stored in confined reservoirs. The major risk associated with geological storage is CO_2 leakage,[10] by slow diffusion through the caprock,[11,12] or through persistent permeable pathways such as tectonic faults in the bedrock.[13] Leakage rates of less than 0.1% are required for a technologically viable storage.[14]

Mineralization reactions of CO_2 with surrounding calcium-, magnesium-, or iron-rich bedrock components hence forming solid carbonates are believed to be an effective way of preventing leakage. This strategy has been demonstrated recently as extraordinarily successful using basaltic and ultramafic bedrocks passivating CO_2 by rapid carbonation under mild hydrothermal conditions.[15–19] Apart from the globally frequent occurrence of this rock type, the reaction with the alkaline rock components, such as CaO, MgO, and FeO, is promoted with the formation of stable carbonate minerals. The extraordinary reactivity with CO_2 is predetermined by the low silica content and even significantly enhanced in the presence of water if compared to any sedimentary bedrock rich in silicate minerals.[20–24]

An equivalent carbonation process aims for an enhanced energy efficiency using CO_2 as reactive gas in thermochemical energy storage (TCES) systems. Reverting a reversible endothermic chemical reaction, stored excess heat can be liberated on demand by the adequate back-reaction. Metal oxides have been reported to react exothermically with moderately pressurized CO_2 under humid conditions, forming the corresponding carbonates at relatively low temperatures.[25] Apart from sustainable binding of gaseous CO_2 permanently stored in the form of stable solid carbonates, the carbonation reaction is strongly exothermic, which enables the heat of reaction to be used for other purposes in the sense of TCES.[26]

G. Gravogl, Prof. C. L. Lengauer, Prof. R. Miletich
Institut für Mineralogie und Kristallographie
University of Vienna
Althanstraße 14 (UZA 2), Vienna 1090, Austria
E-mail: georg.gravogl@univie.ac.at; ronald.miletich-pawliczek@univie.ac.at
Dr. F. Birkelbach
Institute for Energy Systems and Thermodynamics
TU Wien
Getreidemarkt 9, Vienna 1060, Austria
Dr. D. Müller, Prof. P. Weinberger
Institute of Applied Synthetic Chemistry
TU Wien
Getreidemarkt 9, Vienna 1060, Austria
The ORCID identification number(s) for the author(s) of this article can be found under https://doi.org/10.1002/adsu.202100022.

DOI: 10.1002/adsu.202100022

Since CaO is an essential component for both technological applications, the pressure dependency of the relevant carbonation reaction under hydrous conditions was in the focus of this study. Liu et al.[27] provide a comprehensive and detailed overview on the use of CaO as capture material and its performance enhancement for cyclic CO_2 capture. In particular, performance-enhancing treatments by means of chemical substitution and element doping,[28–30] the effect of hydration and the catalytic activity of water and related species have been considered.[31–33] It also includes thermal treatment of the material and changes of the physical properties, which are extensively discussed in literature.[34–36] A more recent review by Sun et al.[37] focuses aside from the already mentioned procedures on the improvement of various synthesis methods of CaO adsorbents[38–40] and surface modifications with various acids.[41,42] The influence of the CO_2 partial pressure on the carbonation of CaO is also discussed. Various studies confirm an increase in the carbon capture capacity of synthetic CaO adsorbents in the range from 0.01 to 9.0 MPa.[43–45] Interestingly, the capture capacity of CaO samples obtained from natural limestone is less influenced by increased CO_2 partial pressure.[46–48] Attempts to improve the poor cycling stability of this reaction system by switching the partial CO_2 pressure instead of temperature failed, however, due to sintering caused by elevated temperatures.[49,50]

In the present study CaO was chosen deliberately as a model compound in order to investigate its carbonation behavior in the low temperature regime under water saturation. As the investigated temperature regime is not relevant for TCES applications the focus of this study lies on the systematic investigation of the reaction at different temperatures and pressures and its potential for CCS applications.

2. Results and Discussion

2.1. Reaction Yields from In Situ Experiments

Using CaO-H_2O-CO_2 as the model system, powder X-ray diffraction (pXRD) allows an in situ observation of the involved crystalline phases under variation of the CO_2 gas pressure ($p(CO_2)$), the temperature (T), and the available H_2O content inside the reaction chamber. p was confined by the bottle pressures of compressed CO_2 gas in cylinders with $p \leq 5.5$ MPa, which is an equivalent of 150–200 m depth in earth.[51] With respect to the CO_2-mineralization in basaltic rocks at shallow depths, the herein investigated temperature range with 298 K ≤ T ≤ 373 K matches realistic conditions.[19]

A notable reactivity of the investigated metal oxides has been observed for TCES already at ambient T,[52] whereas p within this range has been recently reported to have a pronounced influence on the carbonation rate of various alkaline earth oxides.[25] In this study here no other than the known d-spacings of cubic rocksalt-type CaO, brucite-type $Ca(OH)_2$, and rhombohedral $CaCO_3$ have been attributed to the recorded diffractograms. The individual diffraction images are primarily characterized by the sharp diffraction lines of the crystalline phases of the sample material and show only insignificant parasitic diffraction effects originating from components of the reaction chamber (cf. **Figure 1**). Details on the crystallography of the phases involved and complementary information on relevant physical properties are provided in Table S1, Text S1, and Figure S1 in the Supporting Information.

Preliminary reference experiments with variations of the CaO sample type, complementary tests with anhydrous CO_2 or humidification using N_2 instead of CO_2 were also carried out. In addition, individual long-term measurements were performed in order to obtain information on potential changes of the reaction yields beyond the standard duration. Details on the results of these measurements are summarized in Text S2 and in the series of Figures S2–S10 in the Supporting Information.

2.2. Initial CaO to $Ca(OH)_2$ Hydration

In none of the time series CaO was carbonated directly and the formation of $CaCO_3$ always occurred through intermediate $Ca(OH)_2$,[53,54] which therefore has often been used as a direct starting material for the formation of $CaCO_3$ in earlier studies.[55,56] The reactivity of CaO with H_2O was found to follow both the quantity of the available CaO and the concentration of $Ca(OH)_2$, which in turn is strongly dependent on the reaction rate of the subsequent carbonation step. Any attempt to initiate the reaction in an anhydrous system failed (cf. Figure S2, Supporting Information), while the observed initial hydration was even observed under N_2 atmosphere without significant differences when compared to the start of the reaction using CO_2 as pressurizing agent (cf. **Figure 2** and Figures S3 and S4, Supporting Information).

Figure 2 shows the $Ca(OH)_2$ phase content and its variation with time, as affected by the rates of the initial CaO hydration and the subsequent $Ca(OH)_2$ carbonation. Comparing the relative $Ca(OH)_2$ phase proportions at various T only for the lowest T (= 298 K, 323 K) the conversion of CaO to $Ca(OH)_2$ can be resolved properly by the length of the time increments, while at higher T (= 348 K, 373 K) the initial reaction step is apparently too fast. Due to the decreased reaction rate for the CaO-$Ca(OH)_2$ conversion at low T, it allows in particular at 298 K (Figure 2a) to differentiate the influence of the two individual parts, with the decrease of $Ca(OH)_2$ getting more pronounced as $p(CO_2)$ is increasing. As a consequence of slow $Ca(OH)_2$ yield from the initial hydration step, no significant $Ca(OH)_2$ fractions can build up due to the fast conversion to the carbonate phase at $p(CO_2) \geq 3.0$ MPa.

In general, the p effect on just the hydration step appears to have a minor influence compared to T. Nevertheless, increasing $p(CO_2)$ marginally accelerates the formation of $Ca(OH)_2$, as proven by different runs using N_2 as an inert p medium during hydration (cf. Figure S3, Supporting Information). This is most likely attributed to the higher H_2O transportation rate within the system under pressure. Once the actual carbonation process gets triggered after reaching a critical quantity of $Ca(OH)_2$, the $Ca(OH)_2$ content in the sample is immediately decreased again. The lack of detectable $Ca(OH)_2$ fractions in the low T series (Figure 2a,b) originates from the fact that the carbonation reaction accelerated to such an extent, that the intermediate $Ca(OH)_2$ phase is consumed within a shorter time than resolved in this experiment.

In contrast, T reveals the expected significant impact on the reaction rate, as exemplified by a 90% conversion within

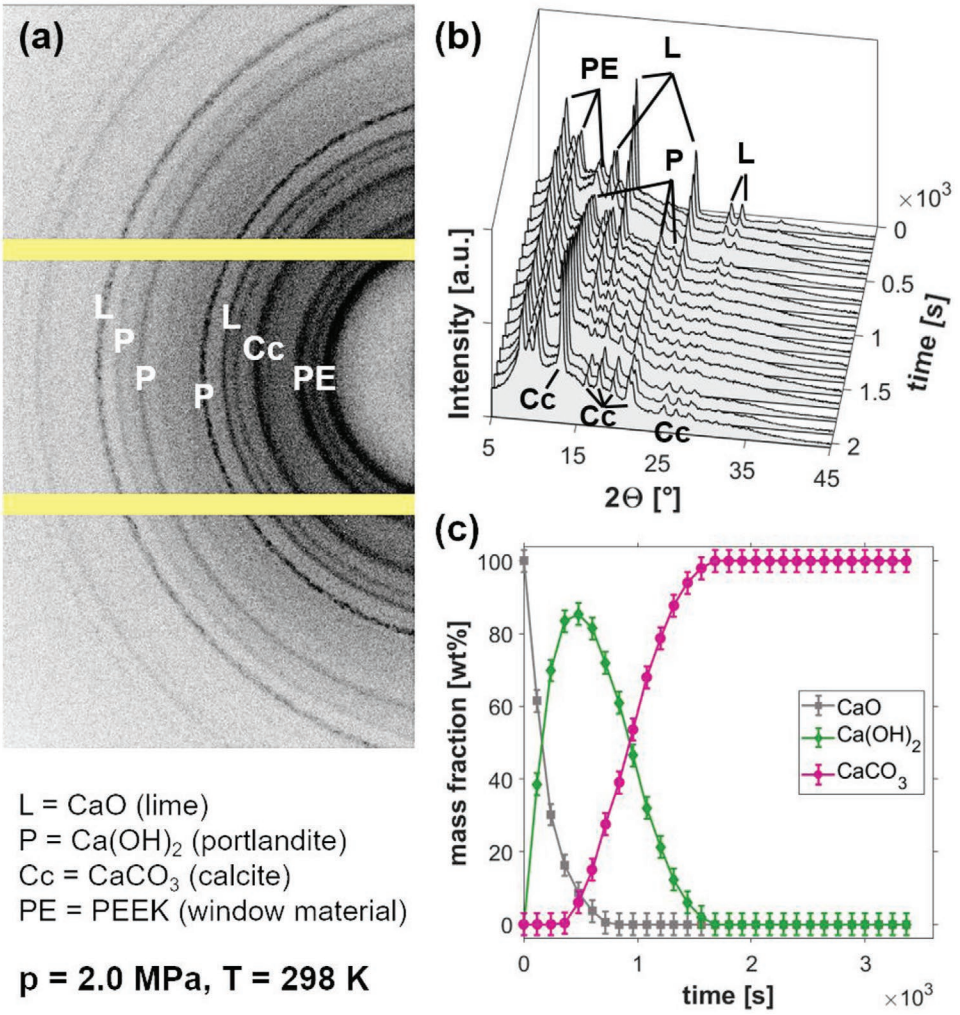

Figure 1. a) Single-frame detector image recorded with a *Pilatus* 300 K pixel detector for 120 s exposure time at the time interval 600–720 s after having initiated the reaction of CaO with $H_2O + CO_2$. b) Time series of integrated powder diffraction profiles within recorded 5°–45° 2θ range as derived from individual single-frame images in a sequence of 17 subsequent measurements within the time period 0–2.04×10^3 s. c) Conversion plots showing relative mass fractions in wt% for each 120 s time interval in a time series of 29 subsequent measurements within 3.48×10^3 s. Vertical error bars correspond to the uncertainties of ±3.0 wt% for determining the mass fractions by means of Rietveld refinement.

less than 480 s already at 323 K. This observation agrees well with the results reported in earlier studies where a notable rate enhancement for the CaO hydration by increasing T and the H_2O partial pressure was observed.[57] When increasing T, a stronger differentiation appears for different $p(CO_2)$ conditions with an inverse relationship between p and T with respect to the $Ca(OH)_2$ proportion in the sample. Increasing $p(CO_2)$ was found in general to decrease the remaining $Ca(OH)_2$ fraction, which is apparently consumed by the formation of the carbonate phase. At higher T, the conversion from the hydroxide to the carbonate appears to be incomplete thus raising the question of a possible kinetic inhibition of the carbonation step.

2.3. Carbonation from $Ca(OH)_2$ to $CaCO_3$

The $CaCO_3$ formation recorded in the time sequences (**Figure 3**) is complementary to the observed $Ca(OH)_2$ mass fraction (Figure 2). The positive effect of $p(CO_2)$ is obvious from the data at 298 K (Figure 3a), thus revealing increasing $p(CO_2)$ to significantly enhance the rate of carbonate formation. These finding fits together well with those relating to the observed $Ca(OH)_2$ fractions, which are reduced to almost insignificant trace contents corresponding to the rapid reaction conversion through CO_2 to the carbonate.

However, the circumstances change under elevated temperatures (323 K), where at low $p(CO_2)$ (i.e., 1.0–3.0 MPa) only partial carbonation (mass fractions < 20 wt%) was achieved, whereas at $p(CO_2)$ of 4.0 and 5.0 MPa maximum carbonation rates have been observed, thus resulting in full conversion of $Ca(OH)_2$ to $CaCO_3$. At even higher T (348, 373 K), a complete reaction conversion could not be achieved in any of the time series up to ≈3.6×10^3 s and the observed mass fractions yield values below ≈35 wt% for $CaCO_3$. Nevertheless, in both experimental series recorded at 348 and 373 K (Figure 3c,d) there is a clear trend toward higher carbonation, which directly scales

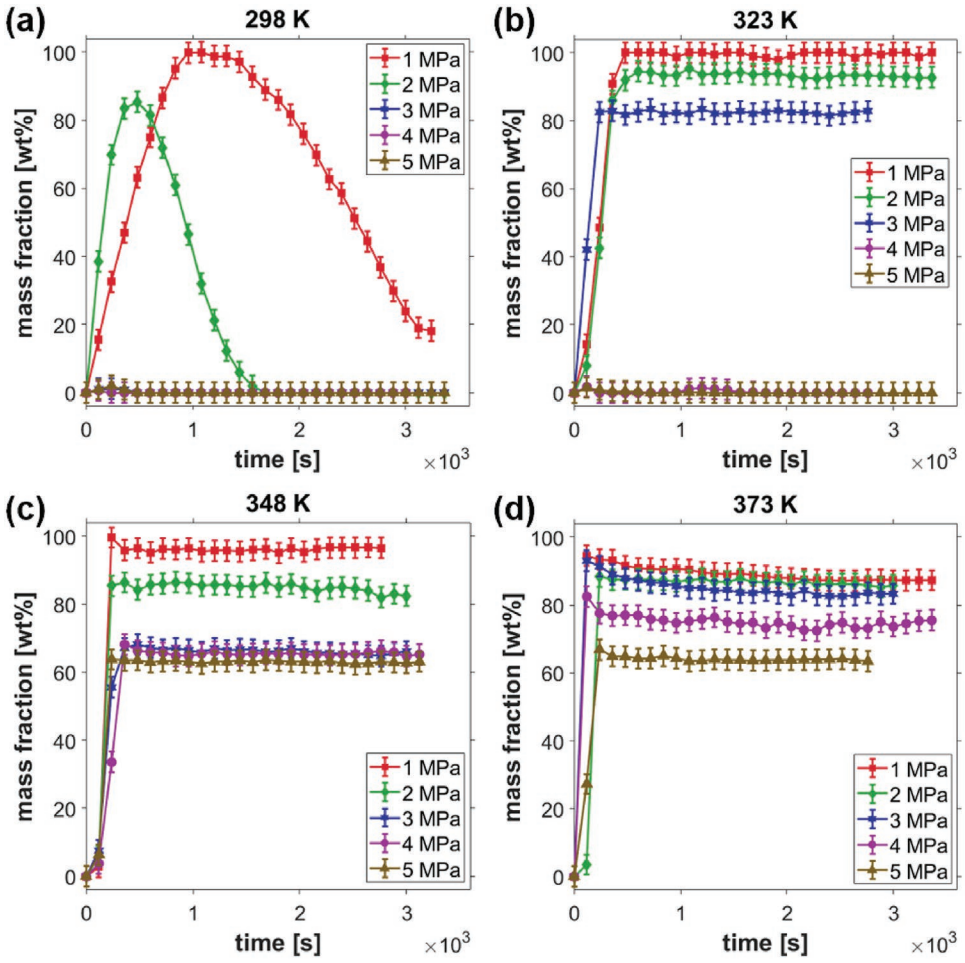

Figure 2. Time series of the relative $Ca(OH)_2$ mass fractions under $p(CO_2)$ variation (1.0–5.0 MPa) at various T: a) 298 K, b) 323 K, c) 348 K, and d) 373 K.

with increasing $p(CO_2)$, though it never exceeds ≈35 wt% $CaCO_3$. Using the preceding CaO-$Ca(OH)_2$ reaction to explain the incomplete conversion appears inappropriate, since for all series the formation of intermediate $Ca(OH)_2$ is fast and identical. The benefit of the even faster carbonation reaction seems no longer valid at higher T, as the carbonation reaction remains incomplete and an apparent equilibrium between $Ca(OH)_2$ and $CaCO_3$ is established without any further changes within the time length of the individual series indicating a kinetic inhibition of the reaction. This finding is further reinforced as the carbonation rates are even higher at low T than at high T when comparing the data at equivalent p conditions (Figure S5, Supporting Information).

A concise mechanism for the formation of carbonates by reaction with gaseous CO_2 and the crucial role of H_2O in this process of carbonation is still pending.[58] In particular, the interaction of hydrous species with respect to the conversion from CO_2 to CO_3^{2-} is under discussion. A common explanation is given by the formation of intermediate carbonic acid H_2CO_3, reacting in form of an acid-base reaction with $Ca(OH)_2$ (Equation (1))

$$\begin{aligned} &H_2O + CO_2 \rightleftharpoons H_2CO_3 \\ &H_2CO_3 + Ca(OH)_2 \rightleftharpoons CaCO_3 + 2H_2O \end{aligned} \quad (1)$$

The hypothesis about carbonic acid as a vital lynch pin for the carbonate formation is supported by reports on carbonic acid proven on $CaCO_3$ mineral particles in tropospheric clouds.[59] Moreover, H_2CO_3 has been stabilized under p, both as a solid but also in aqueous solutions.[60] Experimental data for the CO_2 solubility[61,62] and the calculated[63] solubilities corresponding to the conditions in this study reveal a negative T and a positive p dependency, which matches the carbonate conversion rates found in this study.

2.4. Microstructural Effects

Although apparently contradictory in a first glance, the experiments produce a coherent picture if considering the structure-related factors influencing the reaction progress. As typical for a noncatalytic gas–solid reaction on an interface, apart from I) external and internal mass transport and II) adsorption capabilities of the gaseous species, III) the formation of the product through surface reaction, and IV) diffusion of the reactant through any product layer must be considered.[64] Internal mass transport occurs predominately through pores and along grain boundaries, most likely to a lesser extent by intracrystalline diffusion. External mass transport is negligible, as both H_2O and

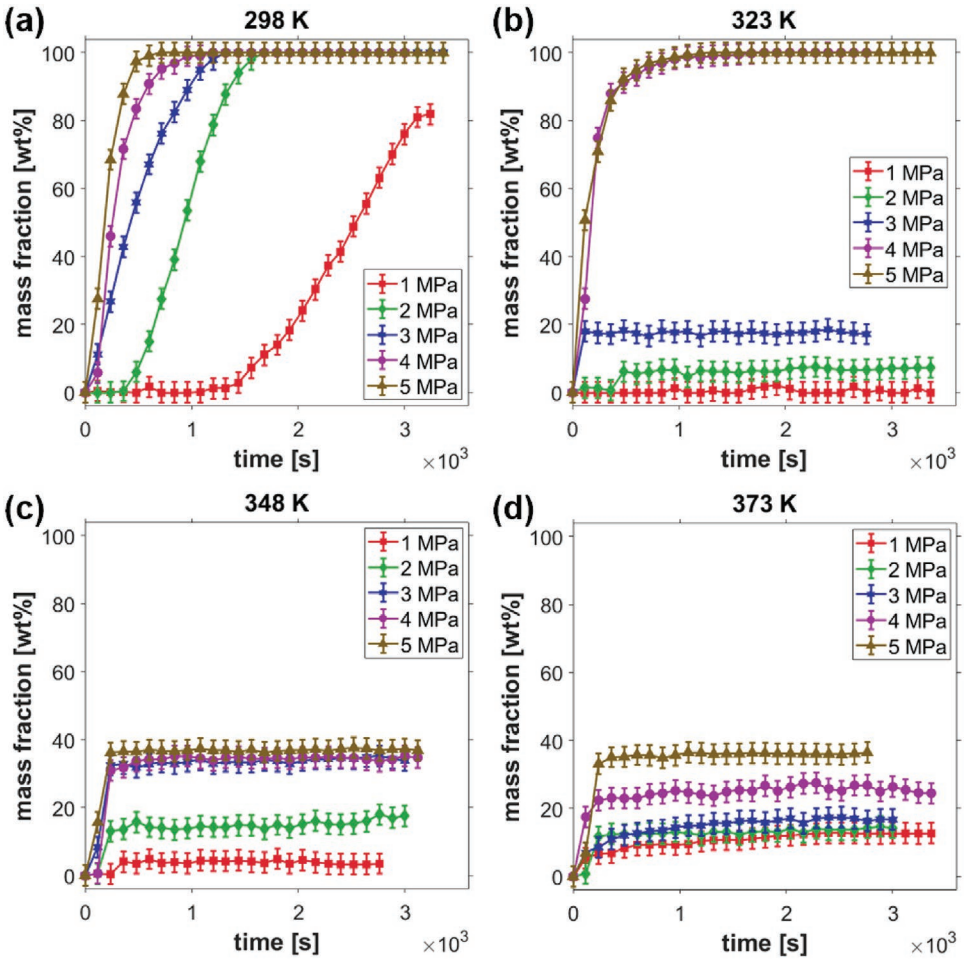

Figure 3. Time series of the relative $CaCO_3$ mass fractions under $p(CO_2)$ variation (1.0–5.0 MPa) at various T: a) 298 K, b) 323 K, c) 348 K, and d) 373 K.

CO_2 are available in sufficient quantities, as demonstrated by the fast conversion rates. Because H_2O was actually present in its liquid state in the reaction chamber, also effects of carbonation under aqueous conditions have to be considered. The first one is the dissolution of CO_2 in H_2O resulting in a mildly acidic environment liberating HCO_3^- and CO_3^{2-} ions V), which are considered as reactive species within this carbonation process.[65] As this effect is the most relevant for the observations gained in this study, the role of H_2CO_3 for the carbonation of $Ca(OH)_2$ is discussed earlier in detail. The effects of leaching of divalent metal ions from a mineral matrix VI) and subsequent precipitation of the corresponding carbonates VII) are discussed later. Generally, the leaching of metal ions from silicates is supposed to be the rate determining step in CCS.[65]

The existence of $Ca(OH)_2$ as an intermediate phase and transient state during carbonation cannot only be explained by the extremely fast reaction of the CaO (100)-surface with H_2O[66] but also volume work and structural changes must be considered. The latter involves major differences in the polyhedral connectivities and the degree of polymerization between CaO_6 building units, structurally determined elastic properties and preferred cleavage, but also large differences of the molar volumes due to the uptake of H_2O and CO_2 as structural components (cf. Text S1, Figure S1, and Table S1, Supporting Information). Considering the uptake of H_2O and CO_2, the volume expansion is significant (i.e., the 54.49 Å^3 volume fraction per Ca atom in $Ca(OH)_2$ and 61.51 Å^3/Ca in $CaCO_3$ compared to 27.95 Å^3/Ca in CaO) thus manifesting volume work by a factor of 1.9 for $Ca(OH)_2$ and 2.2 for $CaCO_3$ relative to that of CaO. Although the extent of volume compression is small within the experimental p range, relative compressibilities (bulk moduli B_0 are 110 GPa for CaO,[67] 33 GPa for $Ca(OH)_2$,[68] and 73.5 GPa for $CaCO_3$[69]) are indicative for the mechanical stabilization at elevated p.

Volume-related changes of the microstructure must be considered referring to the above-mentioned volume work. Accordingly, the growth of $Ca(OH)_2$ particles reduces the original effective pore widths at the particle interfaces as shown in the scheme in **Figure 4**. As a consequence, the permeability for molecular reactants gets reduced and diffusion at grain boundaries and along pore cavities will be significantly hampered. As crystallization is promoted by T, this would explain the observed rate reduction for the carbonation step at elevated T, accompanied by the reduction of the relative permeability compared to less compacted initial CaO starting material.

The increase in volume from CaO to $Ca(OH)_2$ is substantial (+88.9% at ambient conditions), which causes significant mechanical stress at the interface between the $Ca(OH)_2$ reaction

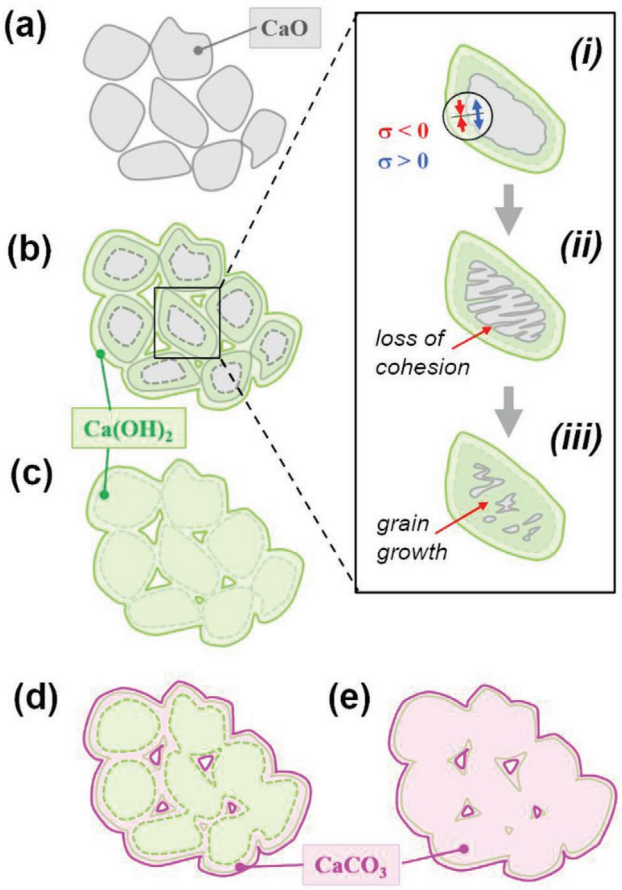

Figure 4. Schematic sequence of the reaction pathway and the microstructural changes involved. a) Loose-packed CaO particles as starting material. b) CaO particles (gray) start reacting to $Ca(OH)_2$ (green) at grain boundaries (c) particles fully hydrated to $Ca(OH)_2$. d) $Ca(OH)_2$ particles (green) with a $CaCO_3$ reaction rim (pink). e) Fully carbonated $CaCO_3$ particles. The image detail shows a single grain with i) corresponding tensile (blue) and compressive (red) stress components at the interface between CaO (= core) and $Ca(OH)_2$ (= rim), ii) the structural loss of cohesion originating from the mechanical stress and the formation of cracks (red arrow) inside the CaO cores, and iii) preferred hydration proceeding along these fracture-plane pathways into the interior of the fragmented crystal grain.

rim and the unreacted CaO core (cf. (i) in Figure 4). This large volume mismatch leads to tensile stress on the unreacted core, from which the loss of structural cohesion and mechanical fragmentation originate (cf. (ii) in Figure 4). This in turn accelerates the progress of hydration of the unreacted CaO core (cf. (iii) in Figure 4).

The equivalent effect can be expected for the subsequent carbonation only that the volume increase from $Ca(OH)_2$ to $CaCO_3$ is just ≈12.8%. Accordingly, the comparable stress components at the interface are significantly lower and might be compensated to a large extent by elastic deformation of the crystal lattices, thus preserving the microstructure in a mechanically metastable state with $CaCO_3$ rims around unreacted $Ca(OH)_2$ cores (cf. Figure 4d). Moreover, the fact that $Ca(OH)_2$ in the grain cores has the larger compressibility compared to $CaCO_3$, the volume mismatch can be easier compensated at higher p. This

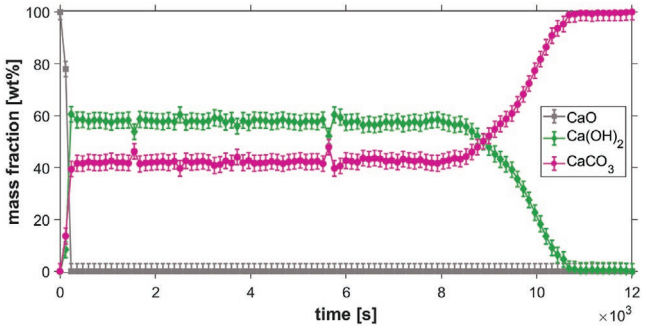

Figure 5. Long time series of up to 12×10^3 s on the reaction progress in the system CaO-H_2O-CO_2 at 348 K and 5 MPa. After a quick initial hydration within less than 400 s, partial carbonation takes place, which appears to be stable and finally lasts for more than 2 h (≈ 8000 s). The complete carbonation step ultimately takes place with a considerable time delay and suggests an associated microstructural change involved.

supports from a perspective of relative lattice properties the role of $Ca(OH)_2$ as intermediate, the activation barrier to shift the equilibrium in the one or other direction being comparably low. That would at least explain the coexistence of the two phases in a certain ratio over a long period of time in the diagrams of Figures 2 and 3. And also, that at higher T the formation of the protective carbonate layer surrounding the $Ca(OH)_2$ cores is forced. At high p conditions the $p(CO_2)$ is high enough to facilitate diffusion through the carbonate surface layer and to diffuse fast enough through the particles, respectively. Due to the enhanced reaction rates at elevated T, a thick protective carbonate layer is formed preventing CO_2 from further carbonation (cf. Figure 3).

This phenomenon is also regularly observed in high T carbonation of CaO for TCES applications.[70] Many studies focus on performance enhancing treatments of the fast, initial stage of carbonation to achieve better reaction yields before the reaction enters the diffusion controlled stage. This is either done by raw material treatments like doping,[71] or optimizing the calcination conditions,[72] but also the effects of T and $p(CO_2)$ on the carbonation are investigated in this context. Similar to the observation within this study, increased $p(CO_2)$ significantly accelerates the reaction kinetics of the carbonation step.[73]

The microstructural bottleneck of a protective layer appears to be rate determining for the carbonation under hydrous conditions, being identical to those described for SrO and BaO.[74] CaO behaves in an equivalent fashion (cf. **Figure 5**), where after rapid initial hydration and a subsequent carbonation step to ≈40 wt% $CaCO_3$ the reaction appears to remain stable for a considerable time, but ultimately the reaction was continued finally yielding 100 wt% $CaCO_3$. The delayed loss of cohesion and the associated relaxation of the stress at the interface then trigger a comparable development, delayed by the metastable maintenance of the microstructure. The spontaneous process can easily be explained by the fact that both phases involved have a pronounced cleavability, which then leads to a comparable fragmentation of the crystallographic structures.

The proposed mechanism of partial fragmentation of the protective carbonate layer, opening new diffusion pathways and finally leading to a full carbonation of the unreacted core is supported by scanning electron microscopy (SEM) pictures after the experiments (cf. **Figure 6**). Figure 6a,b shows a fully

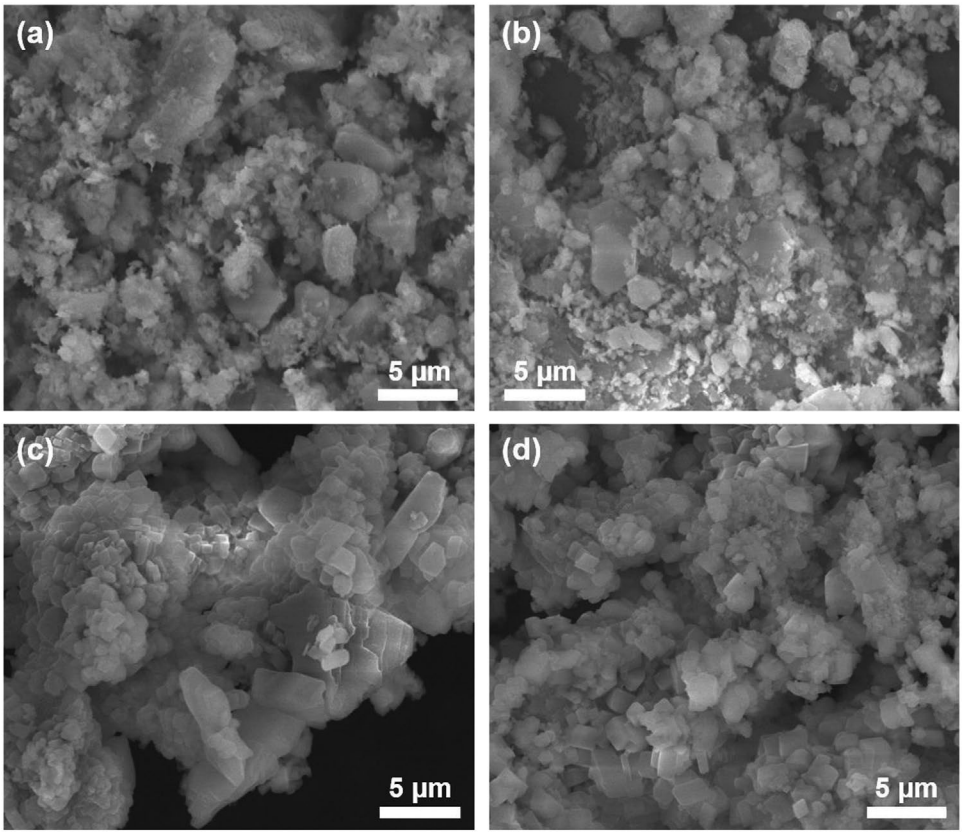

Figure 6. SEM images after various experimental series, showing fully carbonated samples a) after the long time series (12×10^3 s) at 5 MPa and 348 K and b) after the short time experiment (3.6×10^3 s) at 5 MPa and 298 K as well as partly carbonated samples after the short time experiments (3.6×10^3 s) at c) 5 MPa and 348 K and d) 5 MPa and 373 K. Compared to the clean surface in pictures (c) and (d), the more irregular surface in pictures (a) and (b) indicates a partly fragmentation of the carbonate layer opening new diffusion pathways, leading to a carbonation of the unreacted core.

converted sample (100 wt% $CaCO_3$) after the long time series (12×10^3 s) at 5 MPa and 348 K and a short time experiment (3.6×10^3 s) at 5 MPa and 298 K, respectively. In Figure 6c,d, the samples after the short time experiments at 5 MPa and c) 348 K and d) 373 K are shown, representing only partly conversion to $CaCO_3$ at the end of the experimental series. In both cases typical rhombohedral calcite crystal can be seen, but in comparison the surface of the partly converted samples appears to be cleaner and smoother, indicating an intact and nondisturbed carbonate layer. In contrast, the fully converted samples show a more irregular surface with small aggregates between the regular calcite crystals, which is addressed to the proposed partial fragmentation of the carbonate layer, leading to the observed aggregates on the surface.

Regnault et al.[75] investigated the carbonation of $Ca(OH)_2$ with supercritical CO_2 at 16 MPa and temperatures of up to 472 K in the presence of liquid water. The therein reported conversion to $CaCO_3$ matches the results obtained from the low T, high p experiments in this study quite well. They postulated a dissolution and precipitation mechanism, as they found no indication of a protective carbonate layer formed on the $Ca(OH)_2$ surface. This explanation seems not valid for the herein presented carbonation behavior at high T, as the results clearly indicate a kinetic inhibition of the reaction, thus raising the question whether the supercritical CO_2, the different p,T conditions or a combination of both prevent a passivation of the reactive surface.

2.5. Kinetic Evaluation

In order to derive the kinetics of the carbonation reaction, the hydration to $Ca(OH)_2$ as first step (Equation (2))

$$CaO + H_2O \rightleftharpoons Ca(OH)_2 \tag{2}$$

and the carbonation as second step (Equation (3))

$$Ca(OH)_2 + CO_2 \rightleftharpoons CaCO_3 + H_2O \tag{3}$$

are treated separately. The conversion data were processed based on the tensor nonparametric kinetics method, obtaining the effect of selected variables on the reaction rate $d\alpha/dt$ through description with the general kinetic equation (Equation (4))

$$\frac{d\alpha}{dt} = f(\alpha)\ k(T)\ h(p) \tag{4}$$

$f(\alpha)$ represents the effect of conversion α, $k(T)$ the effect of temperature T, and $h(p)$ the effect of the partial pressure p. The

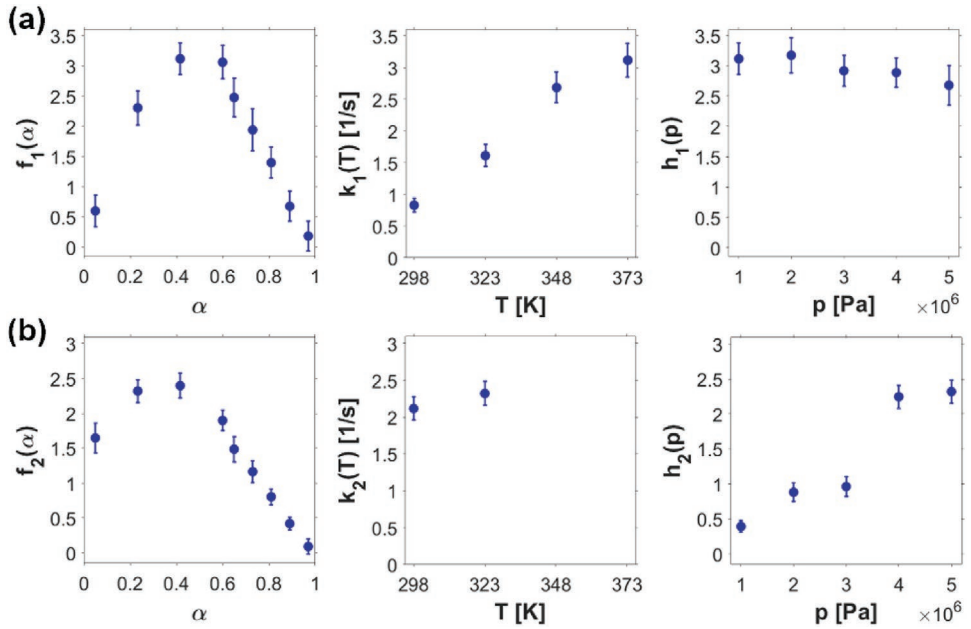

Figure 7. Kinetic model of the reaction in terms of the general kinetic equation with $f(\alpha)$ showing the effect of conversion, $k(T)$ the effect of T and $h(p)$ the effect of p on the reaction rate $d(\alpha)/dt$. a) Hydration part $CaO \rightarrow Ca(OH)_2$ and b) carbonation part $Ca(OH)_2 \rightarrow CaCO_3$. Vertical error bars correspond to the standard deviation of the calculated values.

theoretical background for the applied method is described in refs. [76,77]. With this approach it is possible to extract the effects of k and h for each of the hydration (k_1 *and* h_1) and the carbonation (k_2 *and* h_2) reaction parts, with provided values within their 95% confidence intervals.

For the hydration reaction part (**Figure 7**a) the data yield a very pronounced effect of T, resulting in an increase of the conversion rate by a factor of 3.76 ± 0.94 for the T increase from 298 to 373 K. On the other hand, the effect of p is less pronounced and the conversion rate decreases between 1.0 and 5.0 MPa only marginally by a factor of 0.86 ± 0.21. Since the confidence interval of this factor includes 1, the p effect on the hydration reaction is statistically not significant. It can therefore be concluded that the hydration is almost independent on $p(CO_2)$. Although the T dependency is not strictly linear, the average conversion rate increases with T thus indicating the T sensibility of the reaction. The peak conversion rate ($d\alpha_1/dt$) at 40% conversion increases at a rate of 0.32 ± 0.12 s^{-1} K^{-1} following a simple linear regression, assuming that the variation with p is negligible ($h(p)$ = 2.96 ± 0.15). These results confirm the promotion of the reaction process with increasing T and higher hydration rates at elevated T, as already described in refs. [54,57,66]. The shape of the conversion dependency is typical for a nucleation and growth process in the solid particles.[78]

The second step, i.e., the carbonation reaction part (Figure 7b), is in contrast strongly p dependent with a rate increase by a factor of 5.89 ± 2.12 in the range from 1.0 to 5.0 MPa. The effect of T is associated with a high degree of uncertainty because only data on two T points are available due to the incomplete conversion to $CaCO_3$ at high T. It appears that the effect of T is statistically not significant (factor: 1.1 ± 0.18) and, moreover, the effect of conversion does not match any of the typical models.[78] The average increase of the peak conversion rate ($d\alpha_2/dt$) at 40% conversion can be quantified by a linear fit, which yields 2.56 ± 0.67 × 10^{-6} s^{-1} Pa^{-1}. A shift of the reaction equilibrium toward the side of the reaction products can be clearly seen, with a recognizable acceleration of the reaction rate with increasing $p(CO_2)$, which was also observed in earlier studies.[73]

3. Conclusions and Implications

All individual runs within the experimental series show that the carbonation of CaO in excess of water follows a pathway, which involves intermediate $Ca(OH)_2$. This confirms the inevitably necessary presence of H_2O for the course of the carbonation reaction, as stated by various earlier studies.[27,31,32] The reaction was found to proceed in two-step fashion at all investigated p,T conditions. Our findings provide no evidence for any carbonation under anhydrous conditions, even under maximum $p(CO_2)$, thus following the assumption that $Ca(OH)_2$ is a prerequisite for the reaction with CO_2.[53,54] At the given time resolution it was possible to resolve the hydration from the carbonation steps and to evaluate the influence of p and T independently under the given H_2O saturation. It turns out that the effect of T particularly influences the hydration sub-step (with a variation of $\partial k_1/\partial T$ = 0.032 ± 0.001 s^{-1} K^{-1}), while its influence on the carbonation sub-step is very small. This confirms the earlier findings on the CaO-to-$Ca(OH)_2$ conversion with the preferred binding of H_2O molecules on the (100) surfaces of rock-salt type CaO particles,[66] which in turn also represent the cleavage face of CaO. Great attention must be paid to these mechanical properties, as the huge volume difference between the particle-coating hydroxide product and the unreacted anhydrous cores means that the CaO particles are expected to fragment along these faces and consequently the rapid conversion and the significant T dependency appear plausible.

While the hydration step is only marginally influenced by $p(CO_2)$, there is a significant variation for the carbonation step yielding $\partial h_2/\partial p = 5.0 \pm 0.9 \times 10^{-7}$ s^{-1} Pa^{-1} from the linear fit. An explanation for this p dependency could be the easier stabilization of H_2CO_3 under high p,[60] which should play a major role at the interface structure with respect to the conversion of linear CO_2 molecules to trigonal-planar CO_3^{2-} units due to their steric similarity. Nevertheless, the volume differences are much smaller between $Ca(OH)_2$ particle cores and particle-covering protective $CaCO_3$ layer, which is why the structure at the interface can be mechanically stabilized to some extent. At a given ratio of ≈2:1 the unreacted $Ca(OH)_2$ cores are protected by the encasing $CaCO_3$ layer from a progress of the reaction, unless recrystallization and relaxation of supposed stress occur spontaneously such as observed in other studies.[74]

The p dependency of the carbonation from a hydrated starting material has to be considered for any hydrous system, including mineral reactions of silicates exhibiting a low degree of silicate polymerization. Although the conversion rates should not compare directly with the ones observed in the system CaO-H_2O-CO_2 here in this study, one can expect comparable acceleration of the sub-step involving binding of CO_2 into solid carbonates. With respect to potential silicate phases, such as orthosilicate minerals occurring in basaltic and ultramafic rocks, the rate-determining part is the degradation of the silicate to any hydrated intermediate form, which is the starting point for a similar sub-step as observed for $Ca(OH)_2$ to $CaCO_3$ in this study. With reference to the well-known stabilization of carbonic acid under nonambient conditions, the positive effect of pressure seems to be plausible. Nevertheless, the microstructure including aspects of particle sizes, porosities, and the size of active surfaces are certainly the overriding determinants for the reaction rates. Independent on the other components involved, the demand for sufficient water activity is crucial for the timing of the CO_2 sequestration process and the enhancement of mineralization rates. Similar implications as mentioned for geological CO_2 sequestration apply for thermochemical energy storage applications. Compared to nature there is the advantage of using pure material of tailor-made microstructures, enabling faster carbonation rates than in any natural environment. However, as the reaction needs to occur on timescales less than an hour for feasible TCES applications, the passivating $CaCO_3$-layer becomes a major obstacle, giving a preference for applying high p at low T conditions following the findings reported here. Higher pressure, as geologically applicable by pumping to deeper formations, is not a real technological option for TCES implementation. Concisely summarized, the herein reported results shall contribute to a sustainable climate and energy management delivering appropriate reaction conditions for the carbonation of CaO as model compound for CO_2 fixation in carbon capture applications as well as mechanistic insights into the reaction for CaO-based materials for TCES at higher T.

4. Experimental Section

Starting Materials and Chemical Reactants: The reactions were examined starting from a fine-grained powder sample of CaO (synthetic lime) and using gaseous CO_2 and deionized water. Nitrogen gas was used for neutral reference measurements and helium as a desiccating purging gas. In addition to commercially available CaO (Sigma-Aldrich, 99.9% purity, art. No. 208159), most experiments were carried out using a sample prepared by thermal decomposition from commercial $CaCO_3$ (Sigma-Aldrich, ACS reagent, >99.95 purity, art. no. 398101). CaO was obtained by calcination of the $CaCO_3$ powder at 1173 K for 6.5 h in a muffle furnace (cf. Figure S11, Supporting Information). Both CaO sample types were routinely characterized with respect to phase impurities, crystallinity, average particle size, mean porosity, and specific surface area using standard techniques of pXRD, SEM, and nitrogen physisorption method. Compared to the commercial CaO product, the CaO sample prepared by calcination has a slightly larger porosity and surface area, which appears to be due to the lower calcination temperatures compared to the commercial sample. The CO_2 gas (carbon dioxide 4.5, 99.995% purity, article no. 103040501), N_2 gas (nitrogen 5.0, 99.999% purity, article no. 100542501) and He gas (helium 5.0, 99.999% purity, article no. 102532501) were provided by Messer Austria GmbH and used as supplied without any further treatment.

Analytical Methods: Nitrogen Physisorption: The specific surface area of the two CaO samples was determined by applying nitrogen physisorption technique and performed with an ASAP 2020 instrument from Micromeritics. Each 200–300 mg sample material was degassed under vacuum at 523 K for 12 h prior to the measurement. The surface area was calculated according to Brunauer, Emmett, and Teller and t-plot methods.[79] For the CaO prepared by calcination the specific surface area is 9.11 ± 0.08 m^2 g^{-1}, at a pore volume measuring 0.112 ± 0.009 cm^3 g^{-1} and an average pore width of 501.3 ± 3.4 Å. In contrast, commercial CaO resulted in a surface area of 4.64 ± 0.07 m^2 g^{-1} with a pore volume of 0.043 ± 0.004 cm^3 g^{-1} and an average pore width of 307.4 ± 2.3 Å.

SEM: SEM images (cf. Figure 6 and Figure S12, Supporting Information) were recorded on an FEI Quanta SEM instrument under low-vacuum conditions and in the presence of water vapor in order to prevent electrostatic charging. The samples were mounted on carbon pellets on top of the sample holder and plasma vacuum deposition was used to coat the samples with a thin layer of gold to ensure appropriate conductivity. The gold coating was performed using an AGAR sputtering system at 10 mA for 30 s. The acceleration voltage during the experiments was set to 15 kV. The working distance was 10.4 mm and the spot size on the sample 2.5 nm.

Thermogravimetric Analyses (TGA): In order to determine the approximate content of excess free water in the samples after the experiment, the run products were analyzed with an SDTA851e thermogravimetric analyzer (TGA) from Mettler-Toledo using 70 µL Al_2O_3 crucibles. The samples (about 3–4 mg) were heated up to 383 K with 10 K min^{-1} under a permanent He-gas flow of 20 mL min^{-1}. The target temperature was hold constant for 60 min to ensure that all free water was removed from the run product. The amount of evaporated free water as determined from the weight loss ranges between 40 and 50 wt% for all 15 analyzed samples.

In Situ X-Ray Diffractometry (XRD): XRD Instrumentation: The experimental setup used for all in situ measurements is shown in Figure S13 in the Supporting Information. Figure S13a in the Supporting Information shows the gas-reaction cell made of polyether ether ketone (PEEK), equipped with a resistive heating unit made of stainless steel. Also, the gas inlet and outlet can be seen in this view. Figure S13b in the Supporting Information shows the diffractometer system, an STOE StadiVari goniometer with an open Eulerian cradle, equipped with a Incoatec Mo microsource and a Dectris PILATUS 300 K pixel detector. The whole setup works for diffraction in transmission geometry with the reaction chamber mounted on the Eulerian cradle at chi = 0°. All measurements were carried out in stationary mode ($2\theta = 22°$, $\omega = 0°$) using Mo radiation from an air-cooled Incoatec IµS molybdenum microfocus tube operated at 50 kV/1 mA with a beam diameter of ≈100 µm full width at half maximum on the sample spot.

Sample Environment and Gas-Pressure Cell: The sample was exerted to gas pressures between 1.0 and 5.0 MPa at moderate temperatures, i.e., between room temperature (RT = 298 K) and 373 K inside the

reaction chamber of an adapted gas-pressure reaction cell, modified from the cell type described by Moury et al.[80] All experiments were carried out using 1 mm thick PEEK windows used as X-ray transparent window material. Pressures were controlled by means of a digital manometer to within ± 20 kPa. Temperatures were monitored to within ±0.3 K through a K-type thermocouple directly implemented into the gas-pressure reaction cell. About 1.5 mg CaO powder was placed inside the cylindrically shaped reaction chamber (diameter: 3 mm, height: 1 mm). Deionized water was inserted through the gas capillary by using a Hitachi Chromaster 5160 high performance liquid chromatography pump. After evaporation of the water with a steam generator in a separated supply line, the corresponding valve was opened at a partial pressure twice to that of the CO_2 gas pressure to ensure transportation into the reaction chamber. Because the supply line was not heated and the temperature in the reaction chamber was ≤373 K, the contact between the CaO and hydrous CO_2 pressure medium was achieved with H_2O in the liquid state and under water saturation, in order to ensure a homogenous distribution of the water in the reaction chamber and also within in sample. The condition of saturation was proven by TGA analyses of the samples after each experimental series. Between individual experiments the reaction cell itself but also all adjacent capillaries were purged with pure helium in order to get rid of the residual humidity. A scheme of the experimental setup and more detail on the experimental procedure are provided in Text S3 and Figure S14 in the Supporting Information.

X-Ray Diffraction Time Series: Consecutive pXRD measurements were carried out with laboratory instrumentation recording single-frame detector images at 120 s time resolution. 1D profile lines were integrated from recorded Debye powder rings (Figure 1a) and subsequently refined applying the Rietveld method.[81,82] The scale factors for the individual crystalline phases determined from the applied refinements were converted directly into relative mass fractions (Figure 1c). In total, 20 time series were finally recorded at five different p steps and four distinct T points over a time interval of up to 3.6×10^3 s.

Data Evaluation and Rietveld Refinement: The individual frames with recorded Debye rings were processed using the X-Area 1.72 software from STOE and Cie GmbH software in order to obtain 1D profile lines for subsequent quantitative evaluation. These diffractograms were further evaluated using the PANalytical program suite HighScorePlus v4.5. The phase contents shown in the conversion plots were extracted from relative scale factors for the different phases, as obtained from Rietveld refinements using the routines incorporated in the program suite HighScorePlus v4.5. Details on the XRD data collection strategies, the protocols of pXRD data evaluation and on the refinement strategies are summarized in Text S4 in the Supporting Information.

Supporting Information

Supporting Information is available from the Wiley Online Library or from the author.

Acknowledgements

This work was financially supported by the Austrian Research Promotion Agency (FFG = Forschungsförderungsgesellschaft), Project: 853593. The authors thank Rainer Abart for the discussion on reaction kinetics, Elisabeth Eitenberger and Gernot Friedbacher for performing the SEM analysis, and Claudia Weidenthaler for the cooperation regarding the adaptation of the gas pressure cell.

Conflict of Interest

The authors declare no conflict of interest.

Data Availability Statement

Data available on request from the authors.

Keywords

CO_2 storage, low temperature carbonation, pressure dependence, reaction kinetics, thermochemical energy storage

Received: January 29, 2021
Revised: April 28, 2021
Published online:

[1] S. Yu, P. K. Jain, *Nat. Commun.* **2019**, *10*, 1.
[2] H. Salehizadeh, N. Yan, R. Farnood, *Chem. Eng. J.* **2020**, *390*, 124584.
[3] S. Garcia, S. Kaminska, M. M. Maroto-Valer, *Proceedings of Civil Engineers - Waste and Resource Management* **2010**, *163*, 77.
[4] K. Michael, A. Golab, V. Shulakova, J. Ennis-King, G. Allinson, S. Sharma, T. Aiken, *Int. J. Greenhouse Gas Control* **2010**, *4*, 659.
[5] M. Fujioka, S. Yamaguchi, M. Nako, *Int. J. Coal Geol.* **2010**, *82*, 287.
[6] C. M. White, B. R. Strazisar, E. J. Granit, J. S. Hoffman, H. W. Pennline, *J. Air Waste Manage. Assoc.* **2003**, *53*, 645.
[7] B. Cantucci, G. Montegrossi, O. Vaselli, F. Tassi, F. Quattrocchi, E. H. Perkins, *Chem. Geol.* **2009**, *265*, 181.
[8] L. Chiaramonte, M. Zoback, J. Friedmann, V. Stamp, C. Zahm, *Energy Procedia* **2011**, *4*, 3973.
[9] S. Emberley, I. Hutcheon, M. Shevalier, K. Durocher, B. Mayer, W. D. Gunter, E. H. Perkins, *Appl. Geochem.* **2005**, *20*, 1131.
[10] D. Y. Leung, G. Caramanna, M. M. Maroto-Valer, *Renewable Sustainable Energy Rev.* **2014**, *39*, 426.
[11] A. Hildenbrand, S. Schlömer, B. M. Krooss, *Geofluids* **2002**, *2*, 3.
[12] Z. Li, M. Dong, S. Li, S. Huang, *Energy Convers. Manage.* **2006**, *47*, 1372.
[13] M. A. Celia, J. M. Nordbotten, S. Bachu, M. Dobossy, B. Court, *Energy Procedia* **2009**, *1*, 2573.
[14] P. M. Haugan, F. Joos, *Geophys. Res. Lett.* **2004**, *31*.
[15] E. S. Aradóttir, H. Sigurdardóttir, B. Sigfússon, E. Gunnlaugsson, *Greenhouse Gases: Sci. Technol.* **2011**, *1*, 105.
[16] S. R. Gíslason, H. Sigurdardóttir, E. S. Aradóttir, E. H. Oelkers, *Energy Procedia* **2018**, *146*, 103.
[17] S. R. Gislason, D. Wolff-Boenisch, A. Stefansson, E. H. Oelkers, E. Gunnlaugsson, H. Sigurdardóttir, B. Sigfusson, W. S. Broecker, J. M. Matter, M. Stute, *Int. J. Greenhouse Gas Control* **2010**, *4*, 537.
[18] J. M. Matter, W. Broecker, S. Gislason, E. Gunnlaugsson, E. Oelkers, M. Stute, H. Sigurdardóttir, A. Stefansson, H. A. Alfreðsson, E. S. Aradóttir, *Energy Procedia* **2011**, *4*, 5579.
[19] J. M. Matter, M. Stute, S. Ó. Snæbjörnsdottir, E. H. Oelkers, S. R. Gislason, E. S. Aradottir, B. Sigfusson, I. Gunnarsson, H. Sigurdardottir, E. Gunnlaugsson, *Science* **2016**, *352*, 1312.
[20] I. Galeczka, D. Wolff-Boenisch, E. H. Oelkers, S. R. Gislason, *Geochim. Cosmochim. Acta* **2014**, *126*, 123.
[21] S. R. Gislason, E. H. Oelkers, *Science* **2014**, *344*, 373.
[22] A. P. Gysi, A. Stefánsson, *Geochim. Cosmochim. Acta* **2012**, *81*, 129.
[23] S. O. Snæbjörnsdóttir, S. R. Gislason, *Energy Procedia* **2016**, *86*, 371.
[24] S. O. Snaebjornsdottir, F. Wiese, T. Fridriksson, H. Ármansson, G. M. Einarsson, S. R. Gislason, *Energy Procedia* **2014**, *63*, 4585.
[25] G. Gravogl, C. Knoll, W. Artner, J. M. Welch, E. Eitenberger, G. Friedbacher, M. Harasek, K. Hradil, A. Werner, P. Weinberger, D. Müller, R. Miletich, *Appl. Energy* **2019**, *252*, 113451.
[26] P. Pardo, A. Deydier, Z. Anxionnaz-Minvielle, S. Rougé, M. Cabassud, P. Cognet, *Renewable Sustainable Energy Rev.* **2014**, *32*, 591.

[27] W. Liu, H. An, C. Qin, J. Yin, G. Wang, B. Feng, M. Xu, *Energy Fuels* **2012**, *26*, 2751.
[28] F. D. M. Daud, K. Vignesh, S. Sreekantan, A. R. Mohamed, *New J. Chem.* **2016**, *40*, 231.
[29] Y. Li, C. Zhao, H. Chen, L. Duan, X. Chen, *Fuel* **2010**, *89*, 642.
[30] N. H. Florin, A. T. Harris, *Energy Fuels* **2008**, *22*, 2734.
[31] V. Manovic, E. J. Anthony, *Environ. Sci. Technol.* **2007**, *41*, 1420.
[32] V. Manovic, E. J. Anthony, *Ind. Eng. Chem. Res.* **2010**, *49*, 9105.
[33] P. Sun, J. R. Grace, C. J. Lim, E. J. Anthony, *Ind. Eng. Chem. Res.* **2008**, *47*, 2024.
[34] V. Manovic, E. J. Anthony, *Environ. Sci. Technol.* **2008**, *42*, 4170.
[35] V. Manovic, E. J. Anthony, G. Grasa, J. C. Abanades, *Energy Fuels* **2008**, *22*, 3258.
[36] F. Zeman, *Int. J. Greenhouse Gas Control* **2008**, *2*, 203.
[37] H. Sun, C. Wu, B. Shen, X. Zhang, Y. Zhang, J. Huang, *Mater. Today Sustainable* **2018**, *1*, 1.
[38] Z. Yang, M. Zhao, N. H. Florin, A. T. Harris, *Ind. Eng. Chem. Res.* **2009**, *48*, 10765.
[39] D. Karami, N. Mahinpey, *Ind. Eng. Chem. Res.* **2012**, *51*, 4567.
[40] C. Luo, Y. Zheng, C. Zheng, J. Yin, C. Qin, B. Feng, *Int. J. Greenhouse Gas Control* **2013**, *12*, 193.
[41] F. N. Ridha, V. Manovic, A. Macchi, M. A. Anthony, E. J. Anthony, *Fuel Process. Technol.* **2013**, *116*, 284.
[42] Y. Hu, W. Liu, J. Sun, M. Li, X. Yang, Y. Zhang, X. Liu, M. Xu, *Fuel* **2016**, *167*, 17.
[43] M. Broda, A. M. Kierzkowska, C. R. Müller, *Environ. Sci. Technol.* **2012**, *46*, 10849.
[44] H. Chen, C. Zhao, L. Duan, C. Liang, D. Liu, X. Chen, *Fuel Process. Technol.* **2011**, *92*, 493.
[45] K. Kuramoto, S. Fujimoto, A. Morita, S. Shibano, Y. Suzuki, H. Hatano, L. Shi-Ying, M. Harada, T. Takarada, *Ind. Eng. Chem. Res.* **2003**, *42*, 975.
[46] G. S. Grasa, J. C. Abanades, *Ind. Eng. Chem. Res.* **2006**, *45*, 8846.
[47] C. Salvador, D. Lu, E. J. Anthony, J. Abanades, *Chem. Eng. J.* **2003**, *96*, 187.
[48] A. I. Lysikov, A. N. Salanov, A. G. Okunev, *Ind. Eng. Chem. Res.* **2007**, *46*, 4633.
[49] H. Chen, C. Zhao, Y. Yang, P. Zhang, *Appl. Energy* **2012**, *91*, 334.
[50] J. W. Butler, C. J. Lim, J. R. Grace, *Chem. Eng. Res. Des.* **2011**, *89*, 1794.
[51] D. Turcotte, G. Schubert, *Geodynamics*, 2nd ed., Cambridge University Press, Cambridge **2002**.
[52] D. Müller, C. Knoll, G. Gravogl, W. Artner, A. Werner, J. M. Welch, M. Harasek, R. Miletich, P. Weinberger, *Energy Procedia* **2019**, *158*, 4870.
[53] Z. Li, F. Fang, X. Tang, N. Cai, *Energy Fuels* **2012**, *26*, 2473.
[54] V. Morales-Flórez, A. Santos, I. Romero-Hermida, L. Esquivias, *Chem. Eng. J.* **2015**, *265*, 194.
[55] G. Montes-Hernandez, A. Pommerol, F. Renard, P. Beck, E. Quirico, O. Brissaud, *Chem. Eng. J.* **2010**, *161*, 250.
[56] S. Shih, C. Ho, Y. Song, J. Lin, *Ind. Eng. Chem. Res.* **1999**, *38*, 1316.
[57] E. Serris, L. Favergeon, M. Pijolat, M. Soustelle, P. Nortier, R. S. Gärtner, T. Chopin, Z. Habib, *Cem. Concr. Res.* **2011**, *41*, 1078.
[58] S. F. Wu, T. H. Beum, J. I. Yang, J. N. Kim, *Ind. Eng. Chem. Res.* **2007**, *46*, 7896.
[59] J. Bernard, M. Seidl, E. Mayer, T. Loerting, *ChemPhysChem* **2012**, *13*, 3087.
[60] H. Wang, J. Zeuschner, M. Eremets, I. Troyan, J. Willams, *Sci. Rep.* **2016**, *6*, 19902.
[61] Z. Duan, R. Sun, *Chem. Geol.* **2003**, *193*, 257.
[62] R. Wiebe, V. L. Gaddy, *J. Am. Ceram. Soc.* **1940**, *62*, 815.
[63] L. W. Diamond, N. N. Akinfiev, *Fluid Phase Equilib.* **2003**, *208*, 265.
[64] J. Szekely, J. W. Evans, H. Y. Sohn, *Gas-Solid Reactions*, Academic Press, New York **1976**.
[65] A. A. Olajire, *J. Pet. Sci. Eng.* **2013**, *109*, 364.
[66] P. Liu, T. Kendelewicz, G. E. Brown, G. A. Parks, P. Pianetta, *Surf. Sci.* **1998**, *416*, 326.
[67] S. Speziale, S. R. Shieh, T. S. Duffy, *J. Geophys. Res.: Solid Earth* **2006**, *111*, B02203.
[68] H. Fukui, O. Ohtaka, T. Fujisawa, T. Kunisada, T. Suzuki, T. Kikegawa, *High Pressure Res.* **2003**, *23*, 55.
[69] S. A. T. Redfern, R. J. Angel, *Contrib. Mineral. Petrol.* **1999**, *134*, 102.
[70] Y. Yan, K. Wang, P. T. Clough, E. J. Anthony, *Fuel Process. Technol.* **2020**, *199*, 106280.
[71] L. Andre, S. Abanades, *J. Energy Storage* **2017**, *13*, 193.
[72] B. Sarrion, J. M. Valverde, A. Perejon, L. Perez-Maqueda, P. E. Sanchez-Jimenez, *Energy Technol.* **2016**, *4*, 1013.
[73] C. Ortiz, J. Valverde, R. Chacartegui, L. A. Perez-Maqueda, *ACS Sustainable Chem. Eng.* **2018**, *6*, 6404.
[74] G. Gravogl, C. Knoll, W. Artner, E. Eitenberger, G. Friedbacher, A. Werner, M. Harasek, P. Weinberger, D. Müller, R. Miletich, in *Conf. Proc. ISES Sol. World Congr.*, Abu Dhabi, UAE, 29 Oct.–02 Nov. **2017**.
[75] O. Regnault, V. Lagneau, H. Schneider, *Chem. Geol.* **2009**, *265*, 113.
[76] F. Birkelbach, M. Deutsch, S. Flegkas, F. Winter, A. Werner, *Int. J. Chem. Kinet.* **2019**, *51*, 280.
[77] F. Birkelbach, M. Deutsch, A. Werner, *Renewable Energy* **2020**, *152*, 300.
[78] A. Khawam, D. R. Flanagan, *J. Pharm. Sci.* **2006**, *95*, 472.
[79] S. Brunauer, P. H. Emmett, E. Teller, *J. Am. Chem. Soc.* **1938**, *60*, 309.
[80] R. Moury, K. Hauschild, W. Kersten, J. Ternieden, M. Felderhoff, C. Weidenthaler, *J. Appl. Crystallogr.* **2015**, *48*, 79.
[81] H. M. Rietveld, *Acta Crystallogr., Sect. A: Found. Crystallogr.* **1967**, *22*, 151.
[82] H. M. Rietveld, *J. Appl. Crystallogr.* **1969**, *2*, 65.